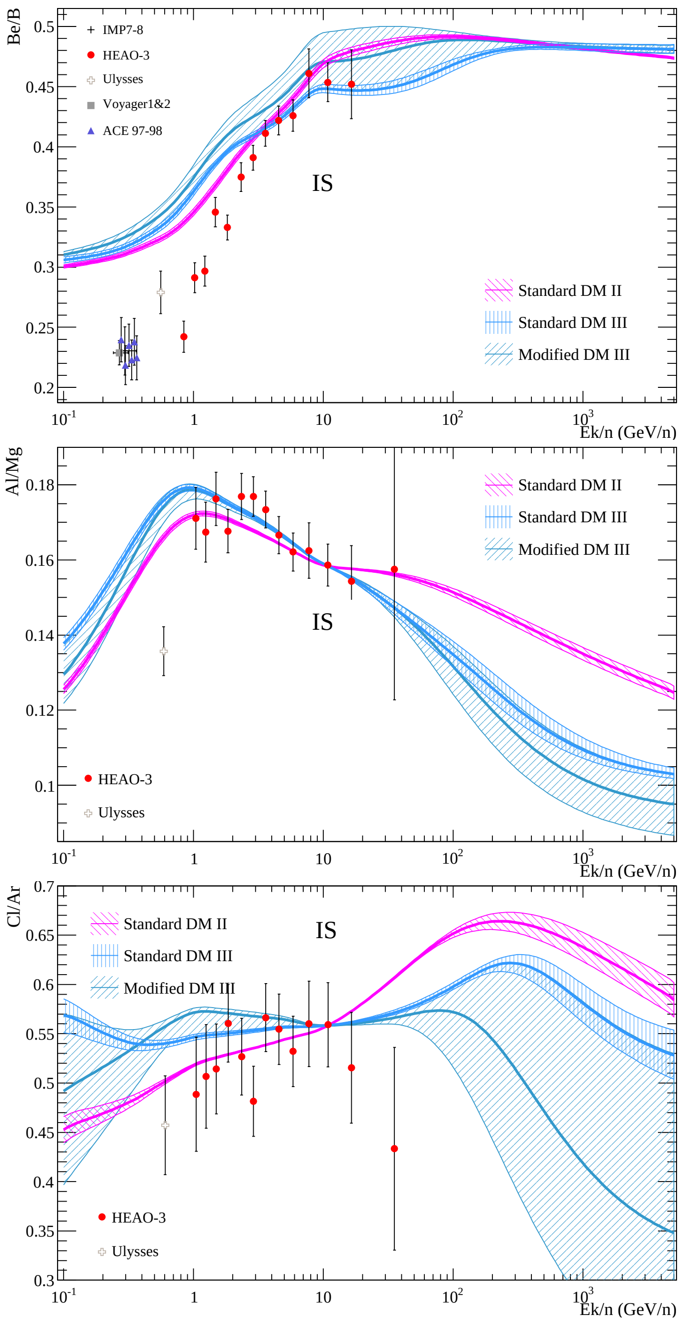

Fig. 13. Same as in Fig. 10 but for the ratios Be/B, Al/Mg, and Cl/Ar.

fitting all these data together: either the model is incomplete or the data themselves may show some inconsistencies. This is more clearly seen from the comparison of the model calculation and the data for these elemental ratios (see below).

5.2.2. Envelopes of 68% CL

From the same set of constraint as in Sect. 5.1.3 (i.e., B/C and the isotopic ratios of radioactive species only), we draw the CL for the elemental ratios in Fig. 13.

Given their large error bars, the elemental ratios are in overall agreement with the data, except at low energy and especially for the Be/B ratio. The main difference between the Be/B ratio and the two other ratios is that Be and B are pure secondary species, whereas all other elements may contain some primary contribution which can be adjusted to more closely match the data. This also explains why the Be/B ratio reaches an asymptotical value at high energy (related to the respective production cross-sections of Be and B), whereas the two others exhibit more complicated patterns. The low-energy Be/B ratio is related to either the model or the energy biases in the production cross-sections for these elements (which is still possible, e.g. Webber et al. 2003), or to systematics in the data. To solve this issue, better data over the whole energy range are required.

5.3. Summary and generalisation to the 2D geometry

Using radioactive nuclei in the 1D geometry, we found that in model II (diffusion/reacceleration), $L \sim 4$ kpc and $r_h \sim 0$, and for the best-fit model III (diffusion/convection/reacceleration), $L \sim 8$ kpc and $r_h \sim 120$ pc. The halo size is an increasing function of the diffusion slope δ, but in model III the best-fit value for r_h remains ~ 100 pc for any $\delta \gtrsim 0.3$. This value agrees with direct observation of the LISM (see Appendix B). Measurement of elemental ratios of radioactive species are not yet precise enough to provide valuable constraints.

For now, there are too large uncertainties and too many inconsistencies between the data themselves to enable us to point unambiguously toward a given model. Moreover, one has to keep in mind that any best-fit model is relative to a given set of data chosen for the fit (see Sect. 4.2). We note that there may be ways out of reconciling the low-energy calculation of the Be/B ratio with present data, e.g., by changing the low-energy form of the diffusion coefficient (Maurin et al. 2010), but this goes beyond the goal of this paper.

All these trends are found for the models with 2D geometry. We calculate in Table 8 the best-fit parameters for the standard model II ($r_h = 0$) and the modified model III ($r_h \neq 0$). The values for the 1D geometry are also reported for the sake of comparison. Apart from a few tens of percent difference in some parameters, as emphasised in Sect. 4.5, some differences are expected if the size of the diffusive halo L is larger than the distance to the side boundary R, which is $d_R = 12$ kpc in the 2D geometry. It is a well-known result that the closest boundary limits the effective diffusion region from where CR can originate (Taillet & Maurin 2003). For model II, L is smaller than d_R. We obtain a smaller than 10% difference for K_0, and a $\sim 30\%$ difference for L. For the modified model III, the halo size has a larger scatter (see previous sections), with $L_{1D}^{\rm best} = 13.6 > d_R$. The geometry is thus expected to affect the determination of L. We find that $L_{2D}^{\rm best} = 4.3$ and that the value of K_0 is thus $L_{1D}^{\rm best}/L_{2D}^{\rm best} \sim 3$ times larger, and V_a is $\sim \sqrt{3}$ times larger than in 1D.

6. Conclusions

We have used a Markov Chain Monte Carlo technique to extract the posterior distribution functions of the free parameters of a propagation model. Taking advantage of its sound statistical properties, we have derived the confidence intervals (as well as confidence contours) of the models for